Geochemical Perspectives Letters

Eclogite xenoliths record a constant ocean oxygen isotope composition for 3 billion years

C. Peshek, Z.D. Sharp, S. Aulbach, F. Viljoen

Supplementary Information

The Supplementary Information includes:

- Triple Oxygen Isotope Systematics
- Methods
- Sample Background
- Theoretical High Temperature Triple Oxygen Isotope Fractionation Calculations
- Closed-system Fluid-rock Modelling of Altered Ocean Crust
- Supplementary Tables S-1 to S-3
- Supplementary Figures S-1 and S-2
- Supplementary Information References

Triple Oxygen Isotope Systematics

Triple oxygen isotope measurements consider both the $\delta^{17}O$ and $\delta^{18}O$ isotope ratios which are defined in per mil notation (‰) as:

$$\delta^{x}O = \left(\frac{R_{sample}}{R_{standard}} - 1\right) \times 1000 \qquad \text{(S-1)}$$

where R_x is the $^{18}O/^{16}O$ or $^{17}O/^{16}O$ or heavy to light isotope ratio. Triple oxygen measurements presented in this work are expressed in linearized form represented by the 'delta prime' notation:

$$\delta'^{x}O = 1000 \ln\left(\frac{\delta^{x}O}{1000} + 1\right) \quad \text{(S-2)}$$

Generally, $\delta^{17}O$ and $\delta^{18}O$ values for terrestrial samples covary in a linear fashion with a slope of ~1/2 and define the terrestrial fractionation line (TFL), which follows the general equation:

$$\delta'^{17}O = \lambda \times \delta'^{18}O + \gamma \quad \text{(S-3)}$$

where λ is the empirically defined best-fit slope and γ is the y-intercept, taken as zero. Small differences from the TFL are the focus of this work, where high-precision measurements allow for deviations from the TFL to be defined using the 'big' delta notation and are reported in per meg given by:

$$\Delta'^{17}O = 1000 \times (\delta'^{17}O_{measured} - \lambda \times \delta'^{18}O_{measured}) \quad \text{(S-4)}$$

In this work λ is given by 0.528 (Sharp *et al.*, 2018).

Methods

Isotope analyses were conducted at the Center for Stable Isotopes (CSI) at the University of New Mexico using the standard laser fluorination technique (Sharp, 1990). The analytical precision, based on in-house San Carlos olivine (SCO) measurements from each run period is ± 0.1 ‰ for $\delta'^{18}O$ and ±8 per meg for $\Delta'^{17}O$ ($n = 25$, 1σ) (Sharp, 1990; Cano *et al.*, 2020; Wostbrock *et al.*, 2020) (Table S-1). Orapa eclogite xenoliths were available as both clean mineral separates and bulk rocks. Where clean separates were not available, the bulk rock samples were crushed with mortar and pestle, sieved, cleaned through several ultrasonic baths, and distilled to remove intermediary veined material surrounding the grains. The cleaned material was dried in a heated oven for 12 + hours to remove all residual water prior to mineral separation. Mineral separates of garnet and clinopyroxene were hand-picked under a binocular microscope, where special attention was taken to choose only the most pristine samples, free of inclusions and altered rinds.

Approximately 2 mg of SCO standard and hand-picked garnet and clinopyroxene mineral separates were loaded into a 44-well nickel plate, where each sample and standard contained its own well. Standards were analysed throughout the duration of each run period to assess any potential drift, ensure proper working conditions of the inlet system and mass spectrometer and to determine the standard error for the eclogite analyses. The in-house SCO

standard (NMSCO) used here was calibrated to Vienna Standard Mean Ocean Water (VSMOW) and Standard Light Antarctic Precipitation (SLAP) (Wostbrock *et al*., 2020). Previous SCO average published from CSI recorded the following TOI values: $\delta'^{17}O$ = 2.716 ‰, $\delta'^{18}O$ = 5.255 ‰, $\Delta'^{17}O$: −58 per meg ± 4 based on λ = 0.528 (Cano *et al*., 2020). The SCO values and average from this work (n = 25) are: $\delta'^{17}O$ = 2.737 ‰, $\delta'^{18}O$ = 5.293 ‰, $\Delta'^{17}O$: −58 per meg ± 8, λ = 0.528.

For the analyses, the nickel plate was loaded into a vacuum chamber 24 hours prior to analysis, evacuated while heated under an external halogen lamp. BrF_5 was introduced to the chamber for 30-minutes to pre-fluorinate the sample chamber prior to analysis, reacting any remaining residual water in the fluorination vacuum line introduced during loading. For each analysis, a sample was heated with a CO_2 laser in the presence of 100 mBar of BrF_5 gas to generate O_2 from the sample. The oxygen was then separated by freezing all unreacted BrF_5 with liquid nitrogen (LN) and purified as it passed across a salt trap, removing any remaining condensable phases. The extracted O_2 was condensed in a zeolite trap at LN temperatures followed by passage in a helium stream through a 6-foot 1/8” diameter 13× molecular sieve gas chromatograph (GC) to separate traces of NF_3 that can have an isobaric interference (NF^+ vs. $^{16}O^{17}O$) at mass 33. $\delta'^{17}O$ and $\delta'^{18}O$ values were measured on a Thermo Fisher MAT 253 Isotope Ratio Mass Spectrometer using a reference gas calibrated to VSMOW and SLAP. Each sample run consisted of 30 iterations, where each iteration consisted of a 26 s collection time separated by a 15 s delay between the reference and sample gas allowing for high precision triple oxygen isotope values to be obtained. Eclogite xenolith mineral separate data are provided in Table S-2.

Sample Background

This work presents new triple oxygen isotope data of eclogite xenolith garnet and clinopyroxene mineral pairs from the Orapa (Or) kimberlite (western margin of the Kalahari craton in Botswana) in combination with recently published triple oxygen isotope measurements of eclogite xenolith mineral pairs from the Roberts Victor (RV) kimberlite and ‘modern’ altered oceanic crust whole rocks drilled from DSDP Hole 504B (McGunnigle *et al*., 2022). The Orapa eclogite xenolith data expand the triple oxygen isotope range from Roberts Victor data ($\delta'^{18}O$: 2-7 ‰) by over +2 ‰, representing a total $\delta'^{18}O$ range of 2-9.5 ‰.

The purpose of combing all datasets was to test the preservation of surficial seafloor alteration in the ancient eclogite xenolith oxygen isotope record. We compared the triple oxygen isotope composition of ancient eclogite xenoliths (RV and Or) to the modern, showing a near exact overlap between both. We designate this overlap as a signature of the surficial origins of eclogite oxygen isotope ratios and use this as evidence for an ocean hydrologically moderated by the same processes in the Archean with the same oxygen isotope composition for the ocean. The RV data extend in $\delta'^{18}O$ from approximately 2-7 ‰, which falls short of the entire range exhibited by the modern data. Based on the RV data alone, the mass balance approach of high and low temperature ocean crust would suggest an ocean slightly

lighter than the modern 0 ‰ (Muehlenbachs and Clayton, 1972). Combining both ancient datasets, the complete range realized for the modern crust is presented.

We used the modern AOC analyses including all sample replicates to fully exemplify the heterogenous variation observed for modern ocean crust alteration (Fig. 1). Two 'high temperature' sample runs are far above the mean for the respective sample and are not included in the shaded region of Figure 1. These samples are 345-U1415J-13R-1, 53-57 (2) and 345-U1415J-13R-1,29-31, with bulk rock average and standard deviation (s.d.) $\Delta'^{17}O$ values of −44 per meg (s.d. ± 16) and -48 per meg (s.d. 0.015), respectively. The outlier values are −7 and−14 per meg, respectively. One entire AOC sample with a $\delta'^{18}O$ value of +14.5 ‰ is excluded as it consists of a relatively greater degree of low temperature weathering then the range represented by the general global eclogite xenolith record (~ +2 to +10 ‰), which overlaps with the combine RV and Or range shown for this work. The global record of eclogite xenoliths shows a single sample (n = 825) has a high $\delta^{18}O$ value of ~ +12.5 ‰ from the Siberian Craton (Korolev *et al*., 2018). This single sample is rare most likely due this greater degree of low temperature weathering also being a rare case for bulk ocean crust as it represents a highly permeable (brecciated) zone with time-extended water-flow. Muehlenbachs (1980) during the original collection of these AOC noted that this sample was are and is not significantly representative of the bulk ocean crust alteration in terms of oxygen exchanged between seawater and rock on an annual basis.

Theoretical High Temperature Triple Oxygen Isotope Fractionation Calculations

Oxygen isotope geochemistry quantifies the abundance ratio of the heavy relative to the light isotopes in a substance relative to a standard. The measurable abundance in two coexisting phases is the foundation of oxygen isotope thermometry but requires equilibrium conditions where the forward and back reactions (rate of oxygen exchange) are equal. $^{17}O/^{16}O$ measurements incorporates a robust understanding of the equilibrium status between two phases and has therefore presented a unique perspective for understanding mass dependent fractionations in natural materials on Earth and in the solar system (Clayton *et al*., 1973; Thiemens, 2006). First-principles density functional theoretical models have been useful for determining the partitioning of oxygen in coexisting minerals pairs (Urey, 1947). Theoretically determined fractionation factors are used in this work to determine the equilibrium triple oxygen isotope partitioning between eclogitic mineral phases, garnet and clinopyroxene, versus olivine (Schauble and Young, 2021). This calculation is used to compare the temperature-dependent fractionation between high temperature minerals equilibrated within the mantle or with a mantle-derived melt with eclogite mineral oxygen isotope values. If garnet or clinopyroxene in eclogitic rocks were altered (metasomatized) by a mantle-fluid or formed via igneous process related to a deep-seated mantle-derived melt, then this solution would reflect their expected triple oxygen isotopic compositions if complete equilibration with the melt has resulted in their precipitation. To determine the expected composition of eclogitic phases equilibrated with a mantle melt, we used the equations of Schauble and Young (2021) to calculate the mineral-mineral fractionations for each phase relative to olivine (forsterite) with a mantle triple oxygen isotope composition: $\delta'^{18}O$ =

5.5 ‰ and $\Delta'^{17}O = -55$ per meg. At 1000 °C, the $1000\ln^{18/16}\alpha_{diopside\text{-}forsterite}$ is + 0.5 ‰ and the $1000\ln^{18/16}\alpha_{grossular\text{-}forsterite}$ is +0.03 ‰ (Fig. 2**)**. It is noted here that diopside and grossular are used to generally represent the common minerals, garnet and clinopyroxene, in eclogite xenoliths. The specific mineral type (*i.e.* omphacite versus diopside) does not significantly affect the results of this study. The $\Delta\Delta'^{17}O$ is +1 and + 0.1 per meg, respectively, essentially well below the precision of our analyses. The garnet-olivine fractionation is within analytical error (Cano *et al*., 2020) while the clinopyroxene-forsterite fractionation is slightly greater and encompasses approximately 10 % of the total range found in the global eclogite xenolith record (Korolev *et al*., 2018).

Closed-system Fluid-rock Modelling of Altered Ocean Crust

Background

The oxygen isotope composition of the ancient global ocean is debated due to the $\delta^{18}O$ values of ancient sediments which are 15 ‰ lower than modern analogues (Perry, 1967). Altered oceanic crust (AOC) is an independent proxy that reflects the isotopic composition of the ocean. The idea that the Archean Ocean was not depleted in ^{18}O relative to the modern was first proposed from the Purtiniq ophiolite (Paleoproterozoic ocean crust) (Holmden and Muehlenbachs, 1993) which showed the same $\delta^{18}O$ variation as modern AOC and argued that a large negative $\delta^{18}O$ shift in the expected composition of altered ocean crust would be observed under an isotopically light ocean. This phenomenon occurs as ocean water reacts with the ocean crust, forming new minerals with an ^{18}O abundance that depends on the initial water value, the fractionation factor (a), and the fluid to rock ratio (F/R).

Following the mass balance approach for fluid-rock alteration in a closed system (Taylor, 1977), we modelled the oxygen isotope composition of AOC as a function of the initial rock, mid ocean ridge basalt ($\delta^{18}O_{rock\text{-}initial}$), the initial water, seawater ($\delta^{18}O_{water\ initial}$), the temperature (°C) of alteration, and the fluid-rock (F/R) ratio or X_W (Eqn. S-5). It is worth pointing out that an open system exchange model differs only in the apparent F/R ratio.

$$\delta_{water\text{-}initial}(X_W) + \delta_{rock\text{-}initial}(1 - X_W) + = \delta_{water\text{-}final}(X_W) + \delta_{rock\text{-}final}(1 - X_W) \quad \text{(S-5)}$$

In Equation S-5**,** $\delta^{x}O_{water\text{-}final}$ is resolvable using the expected equilibrium fractionation, $\Delta^{18}O_{basalt\text{-}water}$:

$$\Delta^{18}O_{basalt\text{-}water} = \delta^{18}O_{rock\text{-}final} - \delta^{18}O_{water\text{-}final} \quad \text{(S-6)}$$

Rewritten as:

$$\delta^{18}O_{water\text{-}final} = \delta^{18}O_{rock\text{-}final} - \Delta^{18}O_{basalt\text{-}water} \quad \text{(S-7)}$$

The equilibrium fractionation for ^{18}O was determined using high-temperature experimental data (Cole *et al*., 1987) and low temperature theoretical fractionations (Zhao and Zheng, 2003). If all the other variables in Eqn. S-5 are known, then X_W can be solved in combination with Eqn. S-7:

$$X_W = \frac{\delta^{18}O_{rock\text{-}final} - \delta^{18}O_{rock\text{-}initial}}{\delta^{18}O_{water\text{-}initial} - \delta^{18}O_{rock\text{-}initial} + \Delta^{18}O_{basalt\text{-}water}} \quad \text{(S-8)}$$

Solving the fluid-rock equation for the modern basalt-water system

Separating low and high temperature AOC into two groups, we can solve the closed system fluid-rock equation for X_W under both conditions (Eqn. S-8). The $\delta^{18}O_{rock\text{-}final}$ used here is the actual measured composition of modern low and high temperature altered ocean crust (Table S-3). The modern solution is used to solve Eqn. S-5 for X_W, the only unknown for the modern. The high and low-temperature values used for our calculations are the minimum and maximum of the average of all modern samples, +1.9 and +9.2 ‰, respectively. By using the minimum and maximum from modern AOC, we can solve the boundary conditions for alternative ancient seawater ($\delta^{18}O_{water\text{-}initial}$) values. The minimum final rock value represents the extent of high temperature alteration while the maximum is for the low temperature. The initial rock in both scenarios is the mantle, 5.5 ‰ (Cano *et al*., 2020), and the initial water is seawater with a $\delta^{18}O$ of 0 ‰. Solutions for the modern X_W values under low and high temperature alteration are outlined below.

Substituting a 50 °C $\Delta^{18}O_{basalt\text{-}water}$ value of +18 ‰ and the respective initial and final rock/water values into Eqn. S-8, the X_W solution for low temperature AOC is 0.3. For the high temperature 300°C X_W solution, $\Delta^{18}O_{basalt\text{-}water}$ of 1 ‰ and X_W is 0.79. Using these values, we rearranged Eqn. S-8 to solve for the $\delta^{17}O$ apparent basalt-water fractionations at low and high temperatures. For this, we used a modern ocean $\Delta'^{17}O$ of 0 ‰ and solved for the $\delta'^{17}O$ value of seawater using Eqn. S-4.

Rearranging Eqn. S-8 to solve for the $\delta^{17}O_{rock\text{-}final}$, we can solve for the apparent fractionation for ^{17}O ($\Delta^{17}O_{basalt\text{-}water}$ in Eqn. S-9):

$$\delta^{17}O_{rock\text{-}final} = X_W\left(\delta^{17}O_{water\text{-}initial} - \delta^{17}O_{rock\text{-}initial} + \Delta^{17}O_{basalt\text{-}water}\right) + \delta^{17}O_{rock\text{-}initial} \quad \text{(S-9)}$$

The low temperature $\Delta^{17}O_{basalt\text{-}water}$ is + 9.4 ‰ and the high temperature is +0.49 ‰.

These fractionation factors for both ^{17}O and ^{18}O can now be used to solve for the modern AOC triple oxygen isotope trajectories for both low and high temperature seawater basalt interaction, shown in Figure S-1.

Altered ocean crust under alternative seawater compositions

Alternative ideas regarding the oxygen isotope composition of the global ocean have been proposed to explain the isotopically light $\delta^{18}O$ of ancient sediments. These samples extend the ocean $\delta^{18}O$ estimate to −15 ‰ for the most extreme scenario if we assume that the Archean Ocean temperatures were like the modern (~25 °C) and that the sediments record pristine $\delta^{18}O$ values. Existing hypotheses for the modern ocean $\delta^{18}O$ value of near 0 ‰ depend on the fluxes of ^{18}O between various oxygen-bearing reservoirs on Earth, which exchange with the hydrological cycle on geologic times scales (Muehlenbachs and Clayton, 1976; Muehlenbachs, 1986). More recently, this idea was quantified for ^{17}O using the additional isotopic system to constrain the two most relevant processes, continental weathering (CW) and high temperature hydrothermal alteration of oceanic lithosphere (HT) which drive the ocean's modern composition and are capable of significantly altering the modern to a lower oxygen-18 abundance (Sengupta and Pack, 2018; McGunnigle *et al*., 2022). Changes in the oceans ^{17}O content relative to the modern are slight, but still produce shifts in the alteration trajectories in triple isotope space.

Continental weathering (CW) is the process whereby low-temperature sediments are formed on the continents, producing ^{18}O enriched rocks relative to typical igneous protolith (evolved relative to MORB) (Muehlenbachs, 1998). The enrichment of ^{18}O in newly formed sediments preferentially incorporates ^{18}O from the hydrosphere, thereby lowering the $\delta^{18}O$ value of the oceans. In the most extreme scenario where CW rates would be 100 times that of the modern, the ocean would be driven to the lowest $\delta^{18}O$ value of −7 ‰ for a steady-state system.

During high-temperature basalt-water interaction, relatively small fractionations between basalt and ocean water result in $\delta^{18}O$ values of altered minerals that are *lower* than MORB, resulting in an increase in the $\delta^{18}O$ value of the ocean. Proposals for a light ^{18}O ocean have considered a lack of HT in the Archean (HT × 0, meaning no seafloor spreading/plate tectonic activity) (Jaffrés *et al*., 2007), resulting in a decrease in the $\delta^{18}O_{ocean}$ modelled here as −4 ‰.

Using both alternative seawater estimates as possible initial ocean water values, the X_W values from the modern solution, and the apparent basalt-water fractionation factors determined for ^{17}O, we solved for the triple oxygen isotope trajectories of MORB altered by seawater of a differing composition than modern (Fig. S-2). Each high and low temperature curve represents the X_W solutions from 0 to 1, with the star along the curve designating the same X_W solutions as the modern, for both low and high temperature alteration. Under a different ocean isotopic composition, the expected range for AOC would fall in between the two green stars (for CW × 100), and between the **X** (mantle) and the purple star (for HT × 0). The latter solution assumes that because high-temperature alteration of AOC is not active, this part of the rock record would not be formed nor observed and should be omitted from the AOC variation. The ancient eclogite samples from Roberts Victor and Orapa show that AOC had nearly the same triple isotope variation in the Archean as the modern and cannot be explained by the other two solutions. This is interpreted as a signature for a similar hydrologic system in the Archean as what exists in the present.

Supplementary Tables

Table S-1 San Carlos olivine standard triple oxygen isotope results collected during eclogite mineral separate analyses. All data are relative to VSMOW2 – SLAP. $\Delta'^{17}O$ values are calculated using a λ of 0.528.

Sample #	$\delta^{17}O$ (‰)	$\delta^{18}O$ (‰)	$\delta'^{17}O$ (‰)	$\delta'^{18}O$ (‰)	$\Delta'^{17}O$ (per meg)
1	2.658	5.157	2.654	5.144	-61
2	2.661	5.156	2.657	5.143	-58
3	2.743	5.326	2.739	5.312	-65
4	2.705	5.260	2.701	5.246	-69
5	2.793	5.390	2.789	5.376	-49
6	2.717	5.260	2.713	5.246	-57
7	2.709	5.233	2.705	5.219	-50
8	2.761	5.331	2.757	5.317	-50
9	2.709	5.243	2.705	5.229	-56
10	2.728	5.278	2.724	5.264	-55
11	2.751	5.317	2.747	5.303	-53
12	2.753	5.312	2.749	5.298	-48
13	2.836	5.498	2.832	5.483	-63
14	2.709	5.243	2.705	5.229	-56
15	2.693	5.207	2.689	5.193	-53
16	2.724	5.304	2.720	5.290	-73
17	2.735	5.279	2.731	5.265	-49
18	2.739	5.278	2.735	5.264	-44
19	2.701	5.244	2.697	5.230	-64
20	2.809	5.457	2.805	5.442	-68
21	2.700	5.228	2.696	5.214	-57
22	2.664	5.199	2.660	5.185	-78
23	2.822	5.461	2.818	5.446	-58
24	2.833	5.474	2.829	5.459	-53
25	2.860	5.546	2.856	5.531	-64
Average	2.741	5.307	2.737	5.293	-58
SD (1σ)	0.056	0.107	0.056	0.106	8

Table S-2 Orapa eclogite triple oxygen isotope results. For each sample, garnet and clinopyroxene mineral separates were analysed when available. All data are relative to VSMOW2 – SLAP. $\Delta'^{17}O$ values were calculated using a λ of 0.528. Per meg is ‰ × 1000. Samples with 1σ values are calculated only for samples with replicate measurements (n > 1).

Sample ID	Phase	n	$\delta^{17}O$ (‰)	1σ	$\delta^{18}O$ (‰)	1σ	$\delta'^{17}O$ (‰)	$\delta'^{18}O$ (‰)	$\Delta'^{17}O$ (per meg)	$\Delta'^{17}O$ 1σ (per meg)
XM3	GNT	2	4.006	0.006	7.719	0.024	3.998	7.689	-62.5	6.4
	CPX	2	4.065	0.078	7.838	0.123	4.057	7.808	-65.5	13.4
766	GNT	2	4.139	0.011	7.979	0.039	4.130	7.947	-65.5	9.2
	CPX	2	3.972	0.194	7.658	0.379	3.964	7.629	-64.5	4.9
XM26	GNT	2	4.230	0.101	8.139	0.172	4.221	8.106	-59.5	10.6
	CPX	2	4.292	0.003	8.313	0.008	4.283	8.279	-88.0	1.4
JJG891	GNT	2	4.610	0.099	8.866	0.194	4.600	8.827	-61.0	2.8
	CPX	2	4.139	0.066	7.986	0.118	4.131	7.954	-69.0	4.2
XM67	GNT	2	4.986	0.161	9.588	0.302	4.973	9.542	-65.0	1.4
	CPX	0	-	-	-	-	-	-	-	-
800	GNT	2	4.302	0.135	8.298	0.266	4.292	8.264	-71.0	4.2
	CPX	2	4.280	0.051	8.263	0.127	4.271	8.229	-74.0	15.6
XM30	GNT	2	4.452	0.055	8.588	0.128	4.442	8.551	-72.5	12.0
	CPX	0	-	-		-	-	-	-	-
XM64	GNT	1	4.959	-	9.540	-	4.947	9.495	-67.0	-
	CPX	1	4.826	-	9.292	-	4.814	9.249	-69.0	-
790	GNT	1	2.677	-	5.148	-	2.673	5.135	-38.0	-
	CPX	1	2.783	-	5.390	-	2.779	5.376	-59.0	-
OE79	GNT	1	3.210	-	6.204	-	3.205	6.185	-61.0	-
	CPX	1	3.007	-	5.835	-	3.002	5.818	-69.0	-
OE81	GNT	1	3.082	-	5.966	-	3.077	5.948	-63.0	-
	CPX	1	2.891	-	5.639	-	2.886	5.623	-83.0	-
OE70	GNT	1	2.526	-	4.851	-	2.523	4.839	-32.0	-
	CPX	1	2.659	-	5.191	-	2.655	5.178	-78.0	-
OE72	GNT	1	2.742	-	5.307	-	2.738	5.293	-56.0	-
	CPX	1	2.866	-	5.563	-	2.862	5.547	-67.0	-
OE86	GNT	2	3.039	0.017	5.903	0.022	3.034	5.886	-73.0	5.7
	CPX	1	2.839	-	5.497	-	2.835	5.482	-59.0	-

Table S-2 continued.

Sample ID	Phase	n	$\delta^{17}O$ (‰)	1σ	$\delta^{18}O$ (‰)	1σ	$\delta'^{17}O$ (‰)	$\delta'^{18}O$ (‰)	$\Delta'^{17}O$ (per meg)	$\Delta'^{17}O$ 1σ (per meg)
OE16	GNT	1	2.487	-	4.791	-	2.484	4.780	-40.0	-
	CPX	1	2.613	-	5.074	-	2.610	5.061	-63.0	-
OE52	GNT	1	2.882	-	5.569	-	2.878	5.554	-54.0	-
	CPX	1	2.782	-	5.412	-	2.778	5.397	-72.0	-
OE18	GNT	1	3.443	-	6.646	-	3.437	6.624	-60.0	-
	CPX	1	3.161	-	6.166	-	3.156	6.147	-90.0	-
789	GNT	1	3.005	-	5.835	-	3.000	5.818	-71.0	-
	CPX	0	-	-	-	-	-	-	-	-
OE83	GNT	1	2.783	-	5.397	-	2.779	5.382	-63.0	-
	CPX	1	2.760	-	5.331	-	2.756	5.317	-51.0	-
787	GNT	1	3.100	-	6.032	-	3.095	6.014	-80.0	-
	CPX	1	2.724	-	5.273	-	2.720	5.259	-57.0	-
OE34	GNT	1	2.412	-	4.655	-	2.409	4.644	-43.0	-
	CPX	1	2.349	-	4.540	-	2.346	4.530	-45.0	-
OE71	GNT	1	2.738	-	5.301	-	2.734	5.287	-57.0	-
	CPX	1	2.880	-	5.608	-	2.876	5.592	-77.0	-
801	GNT	0	-	-	-	-	-	-	-	-
	CPX	1	2.851	-	5.536	-	2.847	5.521	-68.0	-
794	GNT	0	-	-	-	-	-	-	-	-
	CPX	2	2.755	0.162	5.367	0.289	2.751	5.353	-75.0	9.9
OE23	GNT	1	2.673	-	5.170	-	2.669	5.157	-53.0	-
	CPX	2	2.428	0.119	4.690	0.242	2.425	4.679	-45.5	9.2

Table S-3 Modern average minimum and maximum AOC (high and low temperature) triple oxygen isotope data from McGunnigle *et al*. (2022), Table S-2. Isotope values are in per mil (‰) notation relative to the VSMOW-SLAP scale.

Sample Name	T	$\delta^{17}O_{mean}$	$\delta^{18}O_{mean}$	$\delta'^{17}O_{mean}$	$\delta'^{18}O_{mean}$	$\Delta'^{17}O_{mean}$
504B 70 37-1, 36-38	Low	4.82	9.3	4.81	9.24	-0.070
345-U1415J-14G-1 0-6	High	0.98	1.94	0.98	1.94	-0.043

Supplementary Figures

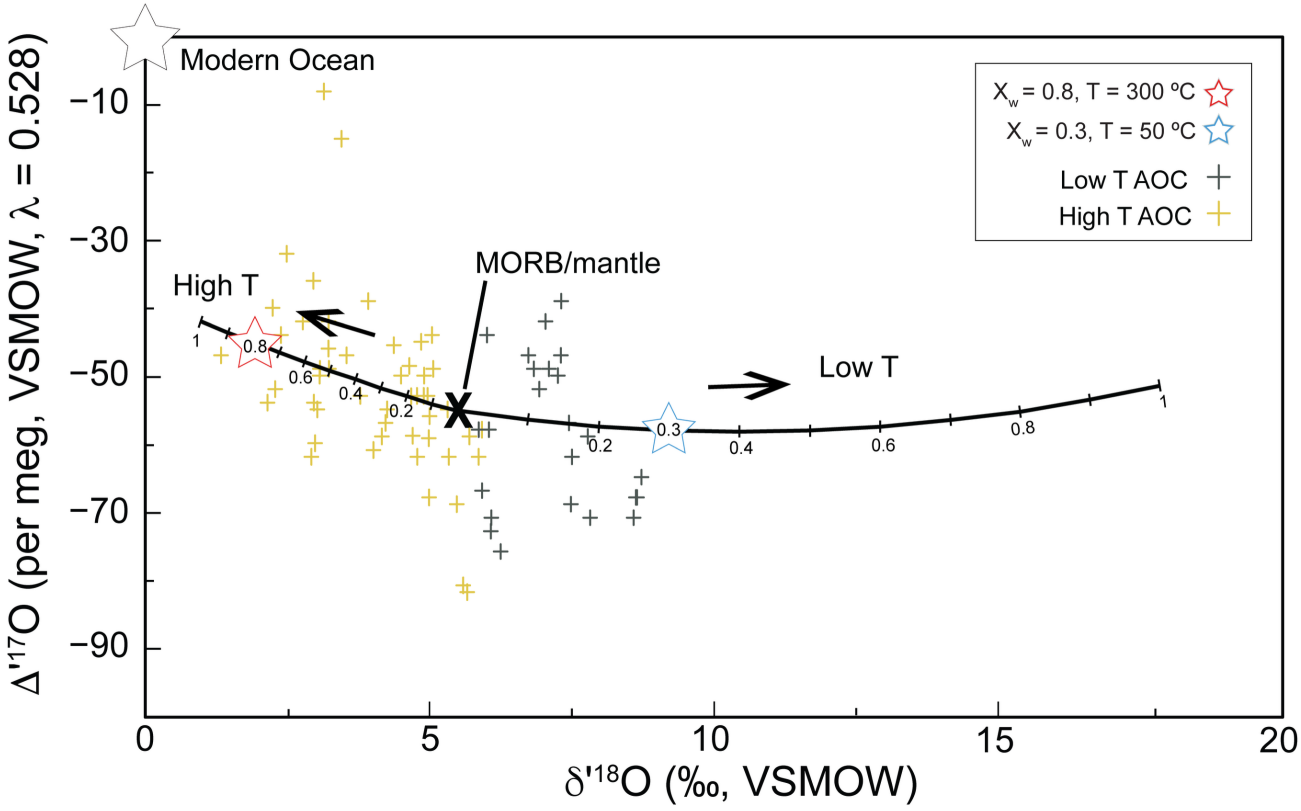

Figure S-1 Triple oxygen isotope alteration of MORB by modern seawater. Closed-system fluid rock alteration of a rock with an initial MORB oxygen isotope composition (**X**) and altered by modern ocean water (white star, black outline) at either low (50 °C) or high (300 °C) temperatures. The alteration trajectories project from the initial rock towards each respective basalt-seawater apparent fractionation, or where X_W = 1 (at the end of each curve). Each dash along the line represents an X_W value or fraction of oxygen from the initial water and rock. The red and blue outlined stars are the final rock solution for the modern (average minimum and maximum AOC) that are used to determine the apparent basalt-water fractionation for ^{17}O.

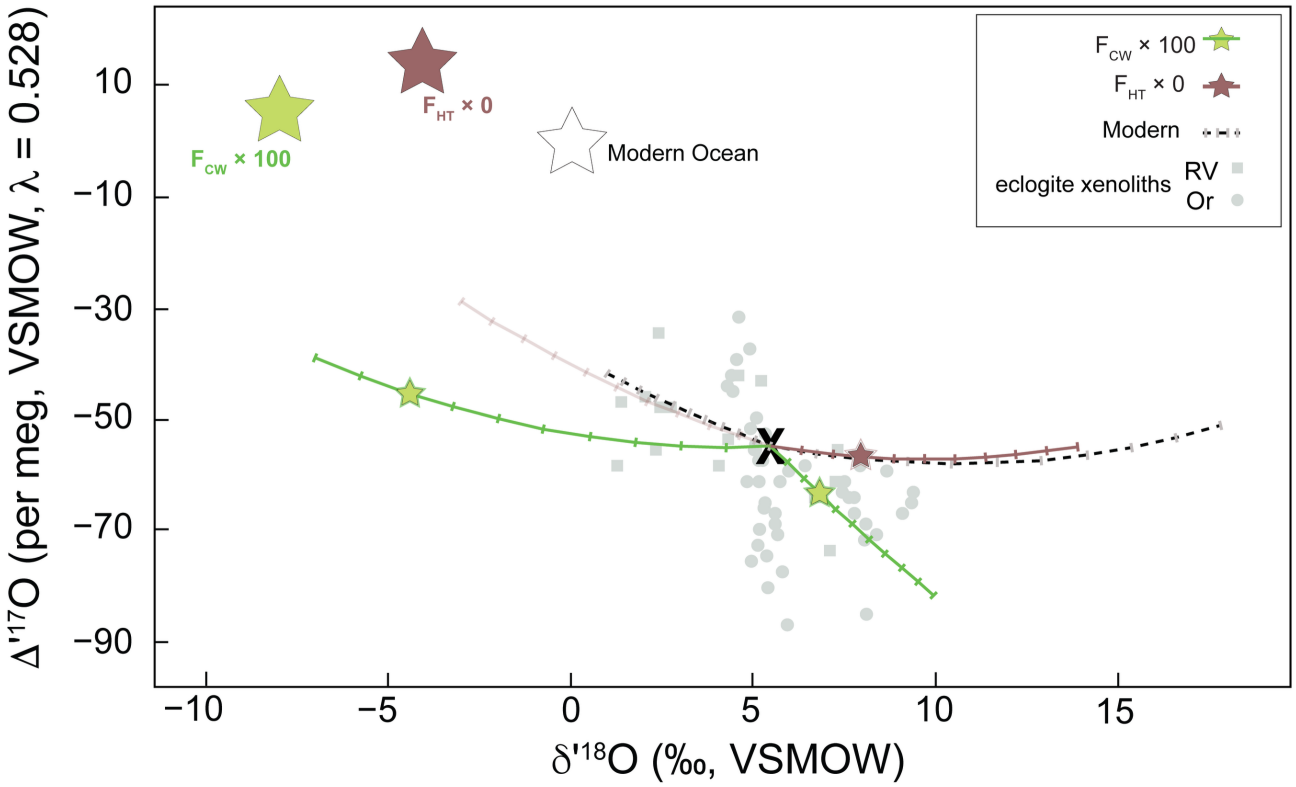

Figure S-2 Solutions for altered oceanic crust under different seawater oxygen isotope compositions: continental weathering times 100 relative to modern (F_{CW} × 100, green curve) and hydrothermal alteration times 0 relative to modern (F_{HT} × 0, purple curve). The stars along the green and purple curves represent the same water fraction (X_W) as the modern solution and serve as the endmembers for the expected range for AOC under each respective ocean. The green curve consists of a high and low temperature range, while the purple only considers low temperature alteration. The black curve shows the solution for the modern (see Fig. S-1 for details). The ocean values used in each model (large stars) were calculated using an adapted form of the steady state model (Muehlenbachs, 1998; McGunnigle *et al.*, 2022). The grey symbols are the ancient eclogite garnet and clinopyroxene data from Orapa (Or, this study) and Roberts Victor (RV). Circles are clinopyroxene, squares are garnet.

Supplementary Information References

Cano, E.J., Sharp, Z.D., Shearer, C.K. (2020) Distinct oxygen isotope compositions of the Earth and Moon. *Nature Geoscience* 13, 270–274. https://doi.org/10.1038/s41561-020-0550-0

Clayton, R.N., Grossman, L., Mayeda, T.K. (1973) A Component of Primitive Nuclear Composition in Carbonaceous Meteorites. *Science* 182, 485–488. https://doi.org/10.1126/science.182.4111.485

Cole, D.R., Mottl, M.J., Ohmoto, H. (1987) Isotopic exchange in mineral-fluid systems. II. Oxygen and hydrogen isotopic investigation of the experimental basalt-seawater system. *Geochimica et Cosmochimica Acta* 51, 1523–1538. https://doi.org/10.1016/0016-7037(87)90334-6

Holmden, C., Muehlenbachs, K. (1993) The $^{18}O/^{16}O$ ratio of 2-Billion-Year-Old Seawater Inferred from Anicent Oceanic Crust. *Science* 259, 1733–1736. https://doi.org/10.1126/science.259.5102.1733

Jaffrés, J.B.D., Shields, G.A., Wallmann, K. (2007) The oxygen isotope evolution of seawater: A critical review of a long-standing controversy and an improved geological water cycle model for the past 3.4 billion years. *Earth-Science Reviews* 83, 83–122. https://doi.org/10.1016/j.earscirev.2007.04.002

Korolev, N.M., Melnik, A.E., Li, X.-H., Skublov, S.G. (2018) The oxygen isotope composition of mantle eclogites as a proxy of their origin and evolution: A review. *Earth-Science Reviews* 185, 288–300. https://doi.org/10.1016/j.earscirev.2018.06.007

McGunnigle, J.P., Cano, E.J., Sharp, Z.D., Muehlenbachs, K., Cole, D., Hardman, M.F., Stachel, T., Pearson, D.G. (2022) Triple oxygen isotope evidence for a hot Archean ocean. *Geology* 50, 991–995. https://doi.org/10.1130/G50230.1

Muehlenbachs, K. (1980) The Alteration and Aging of the Basaltic Layer of Sea Floor: Oxygen Isotope Evidence from DSDP/IPOD Legs 51, 52, and 53. *Initial Reports of the Deep Sea Drilling Project, 51/52/53*, 1159–1167. https://doi.org/10.2973/dsdp.proc.515253.142.1980

Muehlenbachs, K. (1986) Alteration of the Oceanic Crustand the 18O History of Seawater. In: Valley, J.W., Taylor, H.P., O'Neil, J.R. (Eds.) *Stable Isotopes in High Temperature Geological Processes*. De Gruyter, Berlin, 425–444 https://doi.org/10.1515/9781501508936-017

Muehlenbachs, K. (1998) The oxygen isotopic composition of the oceans, sediments and the seafloor. *Chemical Geology* 145, 263–273. https://doi.org/10.1016/S0009-2541(97)00147-2

Muehlenbachs, K., Clayton, R.N. (1972) Oxygen Isotope Studies of Fresh and Weathered Submarine Basalts. *Canadian Journal of Earth Sciences* 9, 172–184. https://doi.org/10.1139/e72-014

Muehlenbachs, K., Clayton, R.N. (1976) Oxygen isotope composition of the oceanic crust and its bearing on seawater. *Journal of Geophysical Research: Solid Earth and Planets* 81, 4365–4369. https://doi.org/10.1029/jb081i023p04365

Perry Jr., E.C. (1967) The oxygen isotope chemistry of ancient cherts. *Earth and Planetary Science Letters* 3, 62–66. https://doi.org/10.1016/0012-821x(67)90012-x

Schauble, E.A., Young, E.D. (2021) Mass Dependence of Equilibrium Oxygen Isotope Fractionation in Carbonate, Nitrate, Oxide, Perchlorate, Phosphate, Silicate, and Sulfate Minerals. *Reviews in Mineralogy and Geochemistry* 86, 137–178. https://doi.org/10.2138/rmg.2021.86.04

Sengupta, S., Pack, A. (2018) Triple oxygen isotope mass balance for the Earth's oceans with application to Archean cherts. *Chemical Geology* 495, 18–26. https://doi.org/10.1016/j.chemgeo.2018.07.012

Sharp, Z.D. (1990) A laser-based microanalytical method for the *in situ* determination of oxygen isotope ratios of silicates and oxides. *Geochimica et Cosmochimica Acta* 54, 1353–1357. https://doi.org/10.1016/0016-7037(90)90160-M

Sharp, Z.D., Wostbrock, J.A.G., Pack, A. (2018) Mass-dependent triple oxygen isotope variations in terrestrial materials. *Geochemical Perspectives Letters* 7, 27–31. https://doi.org/10.7185/geochemlet.1815

Taylor Jr., H.P. (1977) Water/rock interactions and the origin of H2O in granitic batholiths. *Journal of the Geological Society* 133, 509–558. https://doi.org/10.1144/gsjgs.133.6.0509

Thiemens, M.H. (2006) History and applications of mass-independent isotope effects. *Annual Review of Earth and Planetary Sciences* 34, 217–262. https://doi.org/10.1146/annurev.earth.34.031405.125026

Urey, H.C. (1947) The thermodynumic properties of isotopic substances. *Journal of the Chemical Society (Resumed)* 1947, 562–581. https://doi.org/10.1039/jr9470000562

Wostbrock, J.A.G., Cano, E.J., Sharp, Z.D. (2020) An internally consistent triple oxygen isotope calibration of standards for silicates, carbonates and air relative to VSMOW2 and SLAP2. *Chemical Geology* 533, 119432. https://doi.org/10.1016/j.chemgeo.2019.119432

Zhao, Z.-F., Zheng, Y.-F. (2003) Calculation of oxygen isotope fractionation in magmatic rocks. *Chemical Geology* 193, 59–80. https://doi.org/10.1016/S0009-2541(02)00226-7